NPL Report CBTLM 1

September 1999

Stability Limitations In Optical Frequency Standards

P. Taylor

Centre for Basic, Thermal and Length Metrology
National Physical Laboratory
Teddington, Middlesex, TW11 0LW

Abstract

The limiting effects to the stability of optical frequency standards has been assessed. The stability of such a standard depends critically on the spectral width of the atomic absorber. The limiting stability is explored in the absence decoherence (interrogation time limited) and in the more realistic case where optical decoherence and radiative decay are present. The role of motional decoherence in an ion trap system is also discussed.

NPL Report CBTLM 1

ISSN 1469-4921

Authorised for publication on behalf of the Managing Director of NPL by
Steve Manning (Foundation Programme Manager)

Contents

1 Introduction

1.1 Characterisation of a standard

In the assessment of a frequency standard there are three measures by which it can be characterised. These are the standard's stability, reproducibility and accuracy. When describing a frequency standard these three terms have special meanings and can not be used interchangeably.

The *stability* of a frequency standard describes the degree to which the oscillation (or clock) frequency varies over time. A stable oscillator would be one in which all the oscillations were equally spaced in time. However stability says nothing about the actual oscillation frequency of the clock, it simply describes how constant it is. Historically, stability has been achieved using devices from pendulums through hydrogen masers, research grade quartz oscillators to the more recent cryogenic sapphire oscillators and now lasers.

Reproducibility describes the mean frequency difference between an ensemble of frequency standards of the same type. Note that to achieve a particular level of reproducibility requires a stability in excess of that value, but not visa-versa. A good example of this is the hydrogen maser. These devices produce an extremely stable frequency (up to a part in 10^{15} at a few thousand seconds) and yet two devices of the same design can differ in frequency by more than a part in 10^{11} [1]. This is due to collisions between the hydrogen atoms and the microwave chamber in which they reside.

The *accuracy* of a standard describes how well its frequency has been measured relative to the definition of the SI unit of the second *i.e.*[2]:

> ... the duration of 9 192 631 770 periods of the radiation corresponding to the transition between two hyperfine levels of the ground state of the caesium-133 atom.

Frequency standards which are not based on the ground state hyperfine transition of caesium-133 are, by definition, secondary standards and require calibrating. To achieve a particular level of accuracy, requires an equally high reproducibility of the secondary standard. In the case of optical frequency standards, the difficulty of comparing the highly disparate frequencies between optical and microwave tends to lead to optical standards with reproducibilities better than their accuracy. This situation is currently being addressed by the development of more sophisticated frequency comparison techniques (*e.g.* [3, 4, 5]).

1.2 Stability

This report considers only the stability of a frequency standard. It could be argued that stability is the most fundamental requirement for a standard, for without it,

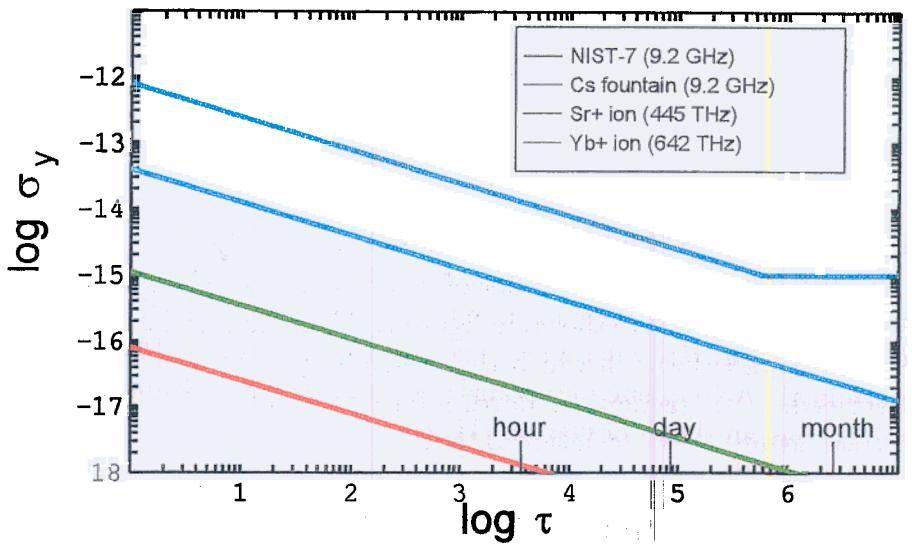

Figure 1: Allan deviation of various Frequency Standards
From the top: NIST-7 currently the world's best caesium beam clock [6], Caesium fountain: the next generation of caesium clock [7], 674 nm transition of a single ion of $^{88}Sr^{+}$ [projected] (0.1 second interrogation time), 467 nm transition of a single ion of $^{171}Yb^{+}$ [projected] (10 second interrogation time)

neither reproducibility nor accuracy can be attained. The stability of microwave frequency standards, particularly that of caesium beam standards is well understood. In these devices the atomic levels involved have effectively infinite lifetime ($\tau_0 \sim$ weeks $\rightarrow$ years) and decoherence effects are low.

In contrast, optical frequency standards are being developed where the upper state lifetime of the clock transition is of the order of a few seconds and a number of sources of decoherence exist. The dependence of the standard's stability on interrogation time, optical decoherence, motional decoherence and radiative decay will all be discussed.

The majority of this report is valid for any optical frequency standard based on cold atom absorbers. There is, however, particular emphasis on optical frequency standards based on single trapped ions. A number of numerical examples are included in the report highlighting the single ion optical frequency standards of strontium and ytterbium which are currently being developed at NPL.

1.3 Allan Variance

The method used to gauge the stability of a frequency standard is the Allan variance [8, 9, 10]. The Allan variance is defined by:

$$\sigma_y^2(\tau) \quad \langle (y_i \quad y_i)^2 \rangle$$

where y_i is the i^{th} frequency measurement sampled over a time τ, and the brackets represent the average over a large number of measurements. The Allan deviation of selected frequency standards are shown in figure 1. The Allan deviation characterises the precision $\delta\omega_{\text{rms}}$ [rad Hz] with which the centre frequency of the clock transition can be determined. A frequency standard, interrogated by a Ramsey interrogation of duration t_{int}, has an Allan deviation [11] of:

$$\sigma_y(\tau) \quad \frac{\delta\omega_{\text{rms}}}{\omega_0} \quad \frac{1}{\omega_0\sqrt{N t_{\text{int}}\tau}} \tag{2}$$

Here ω_0 is the angular frequency of the clock transition, N the number of atoms/ions and τ the sampling time. Though the transition width is not explicit in this expression, it enters implicitly through the interrogation time t_{int} and will be discussed in more depth in chapter 2. As $\sigma_y(\tau) \propto \tau^{-1/2}$ stabilities are often quoted as (say) $10^{-10}\tau^{-1/2}$ to make clear that the stability is white noise limited [10].

Equation 2 also suggests that as $\tau \to \infty$ the stability $\sigma_y(\tau) \to 0$. In fact this is only true until some $1/f$ stability floor is reached. At this point $\sigma_y(\tau)$ levels out and then finally increases. In terms of usefulness as a frequency standard, there is usually little benefit in achieving a stability greatly in excess of the system's reproducibility. The exception to this is when the device is used solely as a short term stable oscillator (*e.g.* the hydrogen maser or a quartz oscillator).

Equation 2 is in fact a rather simplified version of the frequency stability, but it illustrates some interesting points. To minimise $\sigma_y(\tau)$ it is desirable to work at as high a frequency ω_0 as possible, with the most atoms N and for the longest interrogation time t_{int}. These are often contradictory requirements. In caesium fountain microwave standards the relatively low frequency ($\omega_0 \sim 2\pi \times 9.2$ GHz) is counteracted by using large numbers of atoms ($n \sim 10^6$) with $t_{\text{int}} = 1$ s, giving stabilities of $4 \times 10^{-14}\tau^{-1/2}$ [7]. The necessarily large number of atoms give cold collisional shifts which may compromise accuracy. The number of atoms can be reduced if the interrogation time can be increased; this is difficult for a earth based fountain experiment.

In a recent demonstration of a mercury ion microwave frequency standard a slightly inferior stability has been achieved, but using only 7 ions. Due to its higher clock frequency ($\omega_0 = 2\pi\times$ 40.5 GHz) and long interaction times $t_{\text{int}} = 100$ s, a stability of $3 \times 10^{-13}\tau^{-1/2}$ was attained [12]. The use of only 7 ions should lead to

a better reproducibility, as in a linear trap the perturbations to the clock frequency are small and controllable, .

Single ion frequency standards have projected reproducibilities in the parts in 10^{18} region [13]. This is again due to the near ideal environment of the ion trap. However, to achieve this excellent reproducibility on a reasonable time scale ($\tau <$ 1 day), requires a standard with a stability greatly in excess of that which can be achieved with microwave systems. The linear dependence of $\sigma_y(\tau)$ on ω_0 makes a clear case for optical frequency standards. The large increase in ω_0 allows excellent stabilities even for a single ion (N=1). However, it is still necessary to maintain a long interrogation time. As will be discussed later, for most optical frequency standards the lifetime of the clock state places an effective upper bound on the value of $t_{\rm int}$.

As an example of a single ion system consider the $^2S_{1/2}$–$^2D_{5/2}$ 674 nm transition in $^{88}Sr^+$ [14, 4] which has a clock frequency of $\omega_0 = 2\pi \times 445$ THz. Assuming one ion and an interrogation time of 0.1 s (the radiative lifetime of the $^2D_{5/2}$ level is 0.4 s [14, 4]) gives $\sigma_y = 1.1 \times 10^{-15}\tau^{-1/2}$. To reach a stability of 10^{-18} requires $\tau = 1.2 \times 10^6$ seconds, which corresponds to over two weeks.

A similar transition in ytterbium is also being actively pursued as a frequency standard [15, 16]. The $^2S_{1/2}$–$^2D_{3/2}$ 435 nm transition in $^{171}Yb^+$ has a frequency of $\omega_0 = 2\pi \times 680$ THz and a radiative lifetime of 52 ms [17]. With an interrogation time of 13 ms one would achieve a stability of $2.1 \times 10^{-15}\tau^{-1/2}$. The ytterbium system has another transition that is suitable for use as an optical frequency standard. The electric octupole $^2S_{1/2}$–$^2F_{7/2}$ 467 nm transition in $^{171}Yb^+$ [18] has a clock frequency of $\omega_0 = 2\pi \times 642$ THz. It is extremely unusual because the $^2F_{7/2}$ state has a radiative lifetime of 10 years [18]. This makes this optical transition more akin to a microwave transition, in that radiative damping of the $^2F_{7/2}$ state will be negligible. Again assuming one ion, but with a longer interrogation time of one second, (possible because of the effectively infinite radiative lifetime of the $^2F_{7/2}$ level), gives $\sigma_y = 2.5 \times 10^{-16}\tau^{-1/2}$. Here $\sigma_y = 10^{-18}$ is reached at $\tau = 6.3 \times 10^4$s, or 17 hours. This would reduce to less than 2 hours if an interrogation time of 10 seconds could be used.

1.4 Stability limitations

It has already been discussed that $1/f$ noise and reproducibility limitations can set an effective limit on the stability of a frequency standard. This occurs via the maximum averaging time τ at which the Allan variance is still improving. In addition to these limitations, there are also effects which limit the base stability of the system via the maximum interrogation time $t_{\rm int}$that can be used.

One of these factors is the natural lifetime τ_0 of the upper state of the clock transition. Equation 2 is only truly valid in the case where the radiative lifetime

of the clock state is negligible. For most optical systems this is not the case as the clock lifetime is in the range of $\tau_0 \sim 50$ ms $\rightarrow$ 1 s or so. An attempt to increase the interrogation time t_{int} significantly beyond τ_0 will lead to a decrease in the observed signal size and hence the stability. Chapter 3 will discuss this mechanism and other decoherence effects in more detail.

Before this, chapter 2 discusses the ideal case of a system without radiative decay or decoherence, which leads to the derivation of equation 2. This simple case lays the foundation for the rate equation analysis of chapter 3 in the presence of decay and decoherence.

2 Stability in absence of decoherence

This chapter begins with a summary of the basic theory of two-level excitation of a single atom. The theory of Rabi oscillations can then be used to define the correct excitation pulse duration and intensity to achieve the minimum transition width, hence highest Q and stability for a standard. With this in mind, it is then possible to derive the stability for an ideal frequency standard, yielding equation 2. This can be achieved in two ways: the first gives the clearest exposition of the form of the equation; whereas the second, though more involved, allows one to see how the non-ideal case can be added in to the theory. The results of this chapter will then be simply adapted to the more realistic case for an optical frequency standard of a system with a finite radiative lifetime and decoherence. Most of physics described in this chapter is simply a summary from the excellent text "The quantum Theory of Light" by Rodney Loudon [19], which should be consulted if more details are required along with reference [20].

2.1 Rabi Oscillations in absence of decoherence

To begin consider a two level atom with a ground state $|1\rangle$ and an excited state $|2\rangle$ (see figure 2). In this chapter we take the case that the spontaneous emission rate from level $|2\rangle$ to $|1\rangle$ is negligible *. The energy difference between the two levels is equal to $\hbar\omega_0$. The interaction of a *monochromatic* electromagnetic field of angular frequency ω with this two level atom can be described by the optical Bloch equations [19, 21]:

$$\dot{\rho}_{22} = -\dot{\rho}_{11} = i\frac{b^*}{2}\rho_{12}e^{i(\omega_0-\omega)t} + i\frac{b}{2}\rho_{21}e^{-i(\omega_0-\omega)t}$$

$$\dot{\rho}_{12} = \dot{\rho^*}_{21} = i\frac{b}{2}(\rho_{11} - \rho_{22})e^{-i(\omega_0-\omega)t}. \tag{4}$$

Here ρ_{11} and ρ_{22} are the populations of the ground and excited states. The quantity b describes the rate of population transfer between the two states and is known as the Rabi frequency. In the case of an electric dipole (E1) transition, the Rabi frequency b is related to the incident radiation electric field strength E_0 and the atomic dipole matrix element d_e by:

$$b = d_e E_0/2\hbar$$

*This is a physical situation in a microwave frequency standard where the energy separation between the two states is so small that the upper level has a lifetime of many years. In addition the $^2S_{1/2}$–$^2F_{7/2}$ transition in Yb^+ is a good approximation to this model in the absence of decoherence

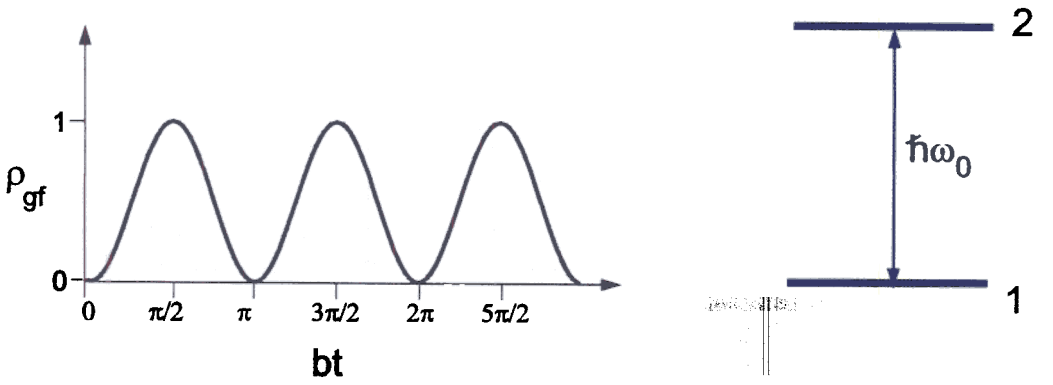

Figure 2: Rabi oscillations at zero detuning
Oscillation is observed for monochromatic light and $b \gg \gamma_0$, where γ_0 is the radiative decay rate of the transition.

Solving the optical Bloch equations with the initial conditions ($\rho_{22} = 0$, $\rho_{12} = 0$) gives the probability ρ_{22} of finding the atom in the excited state (*i.e.* the probability of exciting the transition) after an interaction/interrogation time t_{int} of:

$$\rho_{22} = \frac{b^2}{\Omega^2} \sin^2(\frac{\Omega t_{\text{int}}}{2}) \tag{6}$$

where $\Omega^2 = (\omega_0 - \omega)^2 + b^2$. This is known as the Rabi formula.

With the radiation on resonance with the atomic transition ($\omega = \omega_0$) equation 6 reduces to:

$$\rho_{22} = \sin^2(\frac{1}{2}bt) \tag{7}$$

The population oscillates (or flops) between the two atomic levels governed by the Rabi frequency b (see figure 2). This equation, describing Rabi oscillation of the population is only valid if $b \ll \omega_0$ and $|\omega - \omega_0| \ll \omega_0$ (the rotating wave approximation) (see for example [20] p.357). In addition, it is necessary to emphasise that we have assumed that there is no population decay from the upper level or any dephasing/decoherence events. If we assign a time τ to spontaneous decay or dephasing events then for equation 6 to be valid, we require $b \gg 1/\tau$. The effect of dephasing and population decay will be discussed in the next chapter.

An understanding of Rabi oscillations is important, as it is the mechanism by which population is transfered from one level to another. If the Rabi frequency is known, in principle any excited state population between 0 and 1 can be obtained by varying the quantity bt (often known as the pulse area). As an example of this, if one sets $bt = \pi$ then $\rho_{22} = 1$ (a π pulse) and if $bt = \pi/2$ then $\rho_{22} = 1/2$ (a $\pi/2$ pulse).

2.1.1 Power broadening

An additional consequence of equation 6 is the phenomena of power broadening. If the pulse area is kept fixed and the frequency of the radiation source ω is swept, a Lorentzian line shape is obtained. The full width at half maximum (FWHM) of this line shape is given by FWHM $= 2b$ [radHz]. Hence the observed linewidth of the transition is directly related to the Rabi frequency used. The larger the Rabi frequency, the broader the resulting linewidth.

If one wishes to drive a transition as efficiently as possible, it is necessary to achieve an upper state population of $\rho_{22} = 1$. To achieve this with a single rectangular laser pulse shape therefore requires $bt_{\text{int}} = \pi$. If the pulse area is any greater than π, the width of the transition will be unduly power broadened and will hence be broader than it could have been. This underlies the importance in a frequency standard application of setting the pulse area to its optimum value.

If one sets $bt_{\text{int}} = \pi$ as a fixed parameter, it is easy to see the dependence of the observed transition linewidth on the pulse duration t_{int}. In this case the FWHM is given by:

$$\text{FWHM} = \frac{2\pi}{t_{\text{int}}} \text{ [radHz]} = \frac{1}{t_{\text{int}}} \text{ [Hz]} \tag{8}$$

Hence for the optimum pulse area of $bt_{\text{int}} = \pi$ the width of the transition is inversely proportional to the interaction time. It will be seen later that the stability of the frequency standard depends directly on the transition linewidth. This points to the importance of utilising as long an interaction time as possible so as to minimise the clock transition linewidth and therefore the standard's stability.

2.1.2 Fourier transform limited line shapes

The result of equation 8 can also be obtained from a Fourier analysis of the pulse train. A Fourier analysis is useful, as it allows the effects of more complex pulse trains to be investigated in a straightforward manner.

To excite the atom into state $|2\rangle$ requires a pulse of radiation. This pulse can take many forms, from a single rectangular pulse to Ramsey two-pulse interrogations [22, 23]. The observed line shape in frequency space is simply the Fourier transform of the time domain pulse [24].

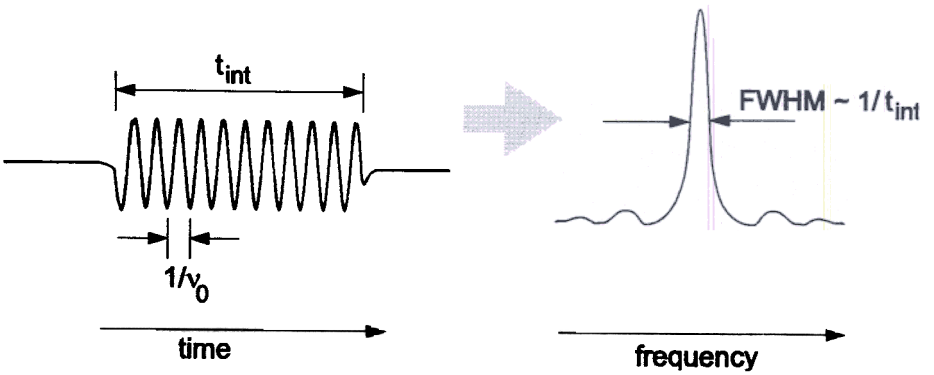

Figure 3: Interaction of a finite pulse train
A truncated monochromatic pulse train of duration $t_{\rm int}$ interacts with an atom. This produces a power spectrum with a central feature of a width dependent on t_{int}

Take for example an atom that is exposed to purely monochromatic radiation of frequency $\nu_0 = \omega_0/2\pi$ for an (interaction) time $t_{\rm int}$ [24]. The atom sees a truncated waveform which in turn leads to a line shape $L(\nu)$ in the frequency domain (see figure 3) given by the Fourier transform of the waveform:

$$\begin{aligned} L(\nu) &= \frac{2}{\pi}\left[\int_0^{t_{\rm int}\nu_0/2} \sin(2\pi\nu_0 t)\sin(2\pi\nu t)\,dt\right]^2 \\ &\approx \frac{2}{\pi}\left[\frac{\sin[(\nu_0-\nu)(\frac{t_{\rm int}}{2})]}{2(\nu_0-\nu)}\right]^2 \end{aligned} \tag{9}$$

This sinc^2 line shape, also shown in figure 3, has a central feature with a FWHM of $0.886/t_{int}$. The numerical factor is for a rectangular pulse and will vary for different pulse shapes. However it is generally true that;

$$\text{FWHM} \approx \frac{1}{t_{\rm int}}\,\text{Hz} \tag{10}$$

This is simply the result as obtained from the Rabi oscillation analysis of equation 8. In order to achieve Fourier transform limited line shapes, however, it is assumed that the pulse area is given by $bt_{\rm int} = \pi$ (a π pulse) as explained by the Rabi oscillation analysis.

A particularly interesting waveform to use is that of a Ramsey interrogation. Here rather than using a single long interrogation of duration $t_{\rm int}$, two shorter pulses

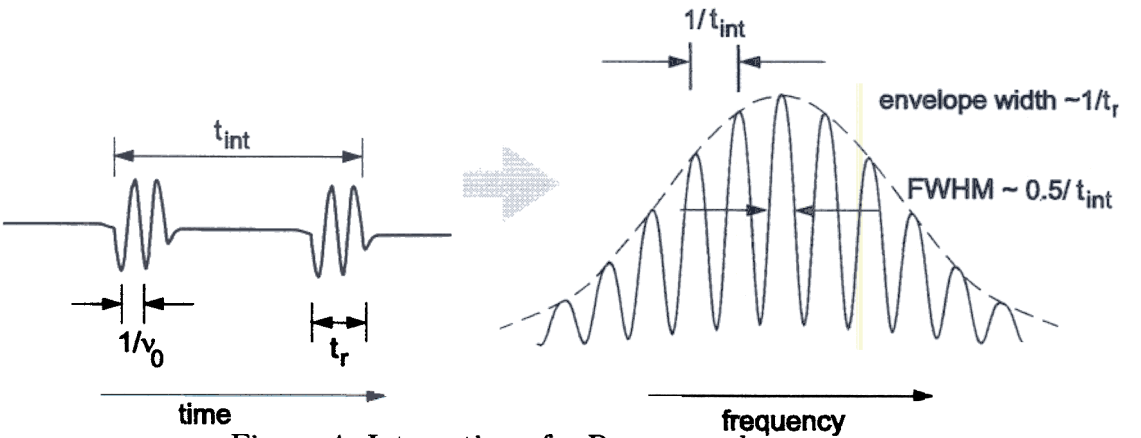

Figure 4: Interaction of a Ramsey pulse sequence
Two monochromatic Ramsey pulses of duration t_r interact with an atom separated by time t_{int}. This produces a set of cosinusoidal Ramsey fringes. The width and separation of these features are related to the free precession time t_{int} whereas the overall envelope is governed by the duration of each of the two Ramsey pulses t_r.

of duration t_r, are used separated by a time t_{int} (see figure 4). Performing a Fourier transform on such a Ramsey pulse gives the well known Ramsey fringes.

The probability of excitation near to line centre is cosinusoidal, given by [23, 24]:

$$\rho_{22} = [1 + \cos(\omega - \omega_0)t_{int}]/2 \tag{11}$$

A set of these Ramsey fringes are formed with separations given by $1/t_{int}$. Each fringe has a FWHM close to $1/2t_{int}$ and the overall envelope has a FWHM of $1/t_r$. Again it is essential that the pulse area is set correctly to achieve these results. A Rabi analysis of Ramsey pulses shows that the two pulses should be of area $\pi/2$ (*i.e.* $bt_r = \pi/2$). The Ramsey interrogation technique was developed for caesium beam standards [25, 23]. In this device the atoms must interact with a microwave cavity and uniform magnetic field over a distance of up to one metre. Using only one pulse of microwave radiation as in figure 3 would lead to broadening of the central resonance due to inhomogeneities in the magnetic field region and phase delays in the microwave cavity [23]. In the case of ion trap standards (where there is no spatial problem) it is unclear whether there would be any significant gain from using a Ramsey style interrogation.

It is particularly important to note that there is nothing particularly magic about the Ramsey interrogation with regards observed linewidth. The central feature is slightly narrower than with a single pulse (0.6 times the single pulse width [22]) but it does not give significantly higher resolution than that obtained by a single pulse

of the same duration t_{int}. It is a common misconception that the Ramsey technique is used to subdivide an atomic line even below the natural linewidth limit. This is not the case.

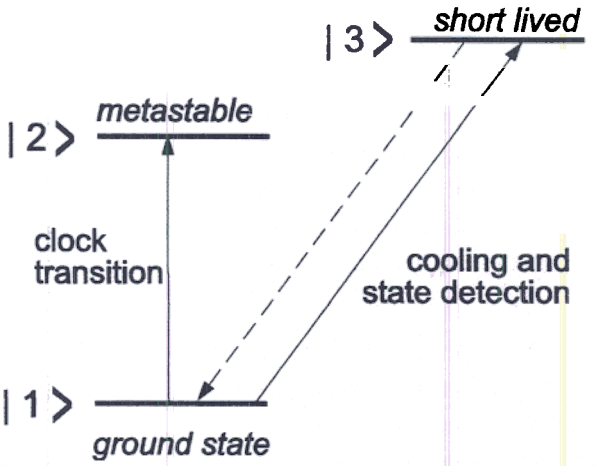

Figure 5: Level structure for a frequency standard

2.2 Quantum projection noise

Quantum projection noise is the fundamental limitation to the stability of an atomic frequency standard and hence also key to the level of reproducibility and accuracy that can be achieved. The noise comes about at the fundamental quantum level, whereby the outcome of a single measurement is indeterminate. Knowledge of a particular variable (say the centre frequency of an atomic transition) is built up by making n measurements. This projection or shot noise has statistical properties and follows a Poisson distribution [26]. It follows that the uncertainty in the measurement of a particular variable (say the uncertainty in the knowledge of the centre frequency $\delta\omega_0$) will decrease with the number of measurements as

$$\delta\omega_0 \propto \frac{1}{\sqrt{n}} \propto \frac{1}{\sqrt{\tau}} \tag{12}$$

where τ is the duration of the experiment (also known as the averaging time).

This section begins with a more detailed discussion of quantum projection noise, including the derivation of the theoretical stability of a frequency standard previously stated in equation 2. This equation is then rederived in a different way, highlighting the importance of the atomic error signal slope. The results of this second derivation are then used in the next chapter to determine the stability of a frequency standard in the presence of radiative decay and dephasing.

2.2.1 Stability of a frequency standard

Consider the common three level system of a frequency standard shown in figure 5. The scheme consists of a ground state $|1\rangle$, a metastable clock state $|2\rangle$ and a short lived excited state $|3\rangle$. The narrow reference transition for the standard lies

between $|1\rangle$ and $|2\rangle$. The strong transition between $|1\rangle$ and $|3\rangle$ is used to cool the atom(s) by the multiple scattering of photons. The scattered light or fluorescence is collected and detected by a sensitive photomultiplier and used to determine the state of the atom(s). With cooling radiation incident an the atom(s), the observation of fluorescence indicates that the atom is cycling between $|1\rangle$ and $|3\rangle$, whereas the absence of fluorescence shows that a clock transition has occured and the atom is in the metastable state $|2\rangle$. Hence the observation/non-observation of fluorescence is a way of determining the state of the atom(s).

The cooling and detection transition is closed; that is to say there is no decay channel from $|3\rangle$ to $|2\rangle$. With a large number of atoms, the level of fluorescence is proportional to the number of atoms remaining in the cooling cycle. This indicates approximately how many atoms have made the transition to the clock state $|2\rangle$. As the level of fluorescence is also dependent on experimental parameters such as the cooling laser power, care must be taken [7]. With only one atom, or a few independently images atoms, the absence of fluorescence from the atom indicates that it is in state $|2\rangle$ with unity probability. Hence, in this case, the state detection is 100% efficient. The laser used to drive the two transitions are gated in antiphase so that the ground state $|1\rangle$ is not broadened by the effect of the cooling radiation.

The principle of operation for all atomic frequency standards is essentially the same. The high Q factor clock transition is probed with a stable oscillator. The oscillator frequency is stepped over that of the atomic transition. At each step the laser is then cooled to detect the amount of fluorescence present, hence the number of atoms that have made the transition to the clock state. In this way a spectra with a narrow line shape is built up. The exact line shape obtained depends on a number of factors, but fundamentally on the interaction time t_{int} as described in the previous section. Common line shapes are Lorentzian (as for a rectangular interrogation pulse) or cosinusoidal Ramsey feature.

In general, to operate as a standard, the interrogating radiation has to be electronically stabilised to the centre of this clock transition. The precision with which this can be achieved $\delta\omega_0$ determines the standard's stability via $\sigma_y(\tau) = \delta\omega_0/\omega_0$. In order to stabilise the oscillator to the centre of the atomic absorption, the transition is probed on either side at frequencies ω_+ and ω_- and the signal level at each of these frequencies is recorded. This is shown in figure 6. The difference in signal from the two sides is used to give an 'atomic error signal'. This allows the determination of the magnitude and direction of the frequency correction required to stabilise the interrogation radiation frequency to ω_0. A minimum measurement cycle therefore relies on interrogating the atom(s) twice, once on each side of the profile.

Consider now the specific case of a Ramsey interrogation of the clock transition between levels $|1\rangle$ and $|2\rangle$ for a single atom. The interrogation sequence sets up a superposition wavefunction ψ of the two states $|1\rangle$ and $|2\rangle$ with weightings c_1 and c_2 respectively such that:

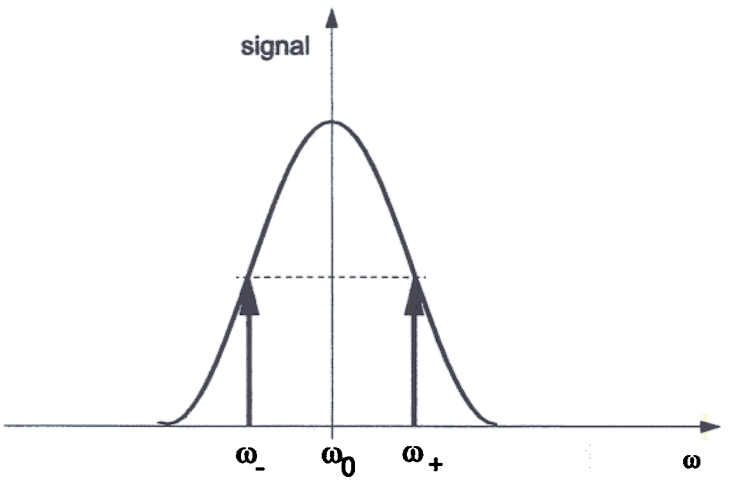

Figure 6: Schematic of stabilisation to an atomic reference line.
The signal level at frequencies ω_+ and ω_- are compared to generate an atomic error signal. The laser frequency is corrected so as to balance the two signal levels.

$$\psi = c_1|1> + c_2|2> \tag{13}$$

After the interrogation, the state of the atom can be determined by driving the detection transition between states $|1\rangle$ and $|3\rangle$. Using the terminology of the Copenhagen interpretation of quantum mechanics, the attempt to detect the fluorescence collapses the wavefunction ψ into either state $|1\rangle$ or $|2\rangle$. If fluorescence is observed, the atom was in $|1\rangle$, if not it was in $|2\rangle$. The probabilities of finding the atom in state $|1\rangle$ or $|2\rangle$ is given by $\rho_{11} = |c_1|^2$ and $\rho_{22} = |c_2|^2$ respectively. Unless c_1 or c_2 are zero, the outcome of the single measurement is uncertain. This is a fundamental feature of quantum mechanics. This uncertainty is called quantum projection noise or shot noise [27].

It is not immediately obvious what the best values of ω_+ and ω_- should be. At the half maxima points of the line shape the slope of the error signal is greatest, but the projection noise greatest. At $\rho = 0{,}1$ the opposite is the case. In fact the precision with which the line centre can be determined $\delta\omega_0$ is independent of the exact values of ω_+ and ω_- used for a cosinusoidal line shape [27] as in this example of Ramsey interrogation. Although a single measurement is indeterminate, if the measurement is repeated n times and/or N atoms are independently interrogated, a more certain result can be achieved.

The previous section stated that the probability of finding the atom in the clock state $|2\rangle$ after the Ramsey interrogation is:

$$\rho_{22} = \frac{1}{2}[1 + \cos(\omega - \omega_0)t_{\text{int}}] \tag{14}$$

where t_{int} is the free precession interrogation time.

The statistical fluctuations in ρ_{22} is given by [27]

$$\Delta\rho_{22} = \sqrt{\rho_{22}(1 - \rho_{22})/N}. \tag{15}$$

For an experiment of total duration τ with N atoms, the total number of data n resulting in the overall measurement is given by $n = N\tau/T$ where T is the time for a single measurement. The uncertainty in the estimated value of ω_0 is thus given by [7]:

$$|\delta\omega_0| = \frac{\Delta\rho_{22}}{|d\rho_{22}/d\omega|} = \frac{1}{t_{\text{int}}}\sqrt{\frac{T}{N\tau}} \tag{16}$$

and hence

$$\sigma_y(\tau) = \frac{1}{\omega_0 t_{\text{int}}}\sqrt{\frac{T}{N\tau}} \tag{17}$$

To obtain the absolute minimum level of shot noise, we need to set $T = t_{\text{int}}$. In this case we allow no time for driving the $|1\rangle$–$|3\rangle$ transition or any other experimental time for switching fields *etc.*. This gives the absolute theoretical minimum stability of a frequency standard as:

$$\sigma_y(\tau) = \frac{1}{\omega_0\sqrt{N t_{\text{int}}\tau}} \tag{18}$$

This is the equation for stability stated in chapter 1.

Hence to obtain the optimum stability it is necessary to minimise the experimental time that is required to prepare states and determine them such that $T \approx t_{\text{int}}$. The above stability has been derived for Ramsey interrogation but can just as easily be derived for arbitrary line shapes by simply substituting in a different expression for ρ_{22}. In these cases very similar results are expected.

2.2.2 Quantum Projection noise for arbitrary line shape

The results of the previous section relate specifically to Ramsey interrogation. No account of line broadening mechanisms was included, the width of the transition being assumed to be the Fourier transform limited width of $\sim 1/t_{\text{int}}$. It is therefore informative to rederive the expression for the projection noise limited stability in a way which will allow us to model the effects of line broadening. This is particularly important if the effects of decoherence are to be included.

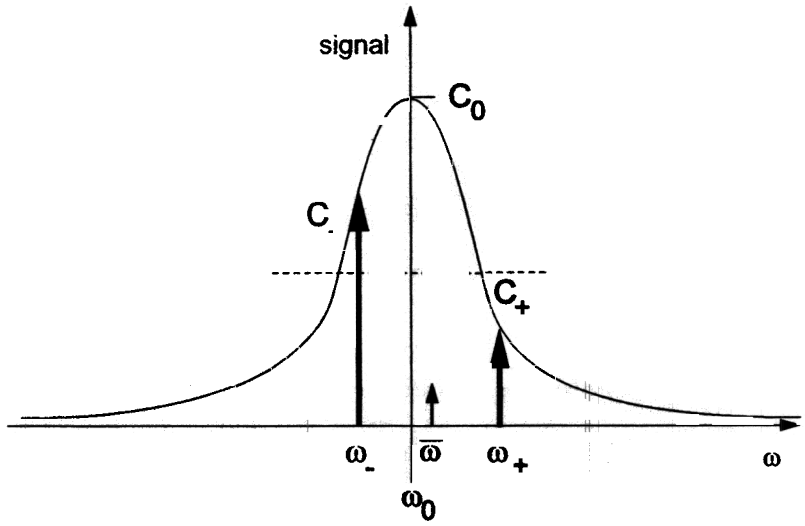

Figure 7: Schematic of stabilisation to an atomic reference line.
The laser frequency is stepped by ±FWHM/2. The signal level $C_\pm$ at these two frequencies $\omega_\pm$ is recorded. The difference between C_- and C_+ is used to generate an atomic error signal, used to servo the mean laser frequency to $\bar{\omega} = \omega_0$

The stability of the standard depends on the precision with which the centre frequency can be determined. In turn, this depends on the slope of the error signal that has been obtained by measuring the signal on the two sides of the clock transition.

In contrast to the previous section, take a clock transition of a Lorentzian shape of figure. This shape results from the Fourier transform of a rectangular pulse shape. In addition, decohering effects which will be discussed in the next chapter tend to also result in Lorentzian line shapes. Such a Lorentzian is shown in figure 7. The signal at line centre ($\omega = \omega_0$) is C_0 and the full width at half maximum is given by $\Delta\omega$ [radHz]. The error signal is derived by recording the signal at two points on either side of the mean frequency $\bar{\omega}$ at ω_+ and ω_- where $C \approx C_0/2$ and taking the difference between these two values. In this case $\omega_\pm \approx \omega_0 \pm$FWHM/2. The slope of the Lorentzian at these points is [24, 26]:

$$\text{slope} = \frac{\partial C}{\partial \cdot} = \frac{C_0}{\Delta \cdot}$$

When the mean frequency is close to ω_0, the signal at ω+FWHM/2 and ω−FWHM/2 on either side of the transition are given by C_+ and C_- respectively:

$$C_+ \quad C_0 \quad \frac{C_0}{\Delta\omega}\left(\frac{\Delta\omega}{2} + \omega - \omega_0\right)$$

$$C_- \quad C_0 \quad \frac{C_0}{\quad}\left(\frac{\Delta\omega}{\quad} \quad (\omega - \omega_0)\right)$$

Hence

$$C_- - C_+ = \frac{2C_0(\omega - \omega_0)}{\Delta\omega} \tag{21}$$

and

$$\omega - \omega_0 = \Delta\omega\frac{(C_- - C_+)}{2C_0} \tag{22}$$

It is worth noting equation 22 differs for a cosinusoidal Ramsey feature by a factor of $\pi/2$ giving, in that case, $\omega - \omega_0 = \Delta\omega(C_- - C_+)/\pi C_0$.

It is now necessary to calculate the uncertainty to which the value $\omega - \omega_0$ can be determined. The uncertainty $\delta\omega_{\text{rms}}$ is given by:

$$\delta\omega_{\text{rms}} = \Delta\omega\frac{\sqrt{\delta C_-^2 + \delta C_+^2}}{2C_0} \tag{23}$$

$$= \frac{\Delta\omega}{2\sqrt{C_0}} \tag{24}$$

as $\delta C_\pm = \sqrt{C_\pm} \approx \sqrt{C_0/2}$.

One measurement cycle consists of two interrogations of duration t_{int}, so that at time $\tau = 2t_{\text{int}}$ the stability is:

$$\sigma_y(\tau = 2t_{\text{int}}) = \frac{\delta\omega_{\text{rms}}}{\sqrt{2}\omega_0} = \frac{\Delta\omega}{2\omega_0\sqrt{2C_0}}. \tag{25}$$

The stability improves with the number of measurements n by the factor $1/\sqrt{n}$. The number of measurements is given by $n = \tau/2t_{\text{int}}$ where, to reiterate, τ is the duration of the measurement. This gives

$$\sigma_y(\tau) = \frac{\Delta\omega}{2\omega_0\sqrt{C_0}}\sqrt{\frac{t_{\text{int}}}{\tau}} \tag{26}$$

This expression is generally valid for a Lorentzian line shape. To obtain the stability for a Ramsey pulse of the previous section (equation 17) we include the factor of $\pi/2$ that differs for the two error signals and note from section 2.1.2 that for a Fourier limited Ramsey pulse $\Delta\omega = 2\pi \times 1/2t_{\text{int}}$. In addition we note that for multi atom experiments $C_0 = N$ where N is the number of detected atoms.

The derivation of equation 26 has important consequences. By not simply assuming that the transition linewidth is Fourier limited (i.e. $\Delta\omega = 2\pi/t_{\text{int}}$), we can see that the stability is directly proportional to the linewidth of the clock transition. Hence any influence which broadens the transition, will also degrade the stability. As will be discussed in the next chapter, there are many effects that homogeneously broaden a transition, including elastic collisions, fluctuating electric and magnetic fields, laser linewidth *etc.* In addition, equation 26 shows that there is a dependence of the stability on the size of the signal. Therefore anything which causes a reduction in signal size (such as radiative decay) will impact adversely on the stability.

3 Decoherence and radiative damping

We have seen so far that an atomic frequency standard is realised by the stabilisation of a local oscillator to the half maxima points of an atomic reference transition. The stability of the standard is governed by the slope of the atomic error signal, *i.e.* the intensity of the signal and its frequency width. Any process which degrades either of these two quantities will necessarily degrade the stability of the standard.

There are many ways in which the clock transition can be perturbed. These mechanisms can be grouped under the headings: radiative damping; optical dephasing; motional dephasing and motional heating. The last two of these mechanisms are solely present in ion trap frequency standards. A detailed discussion of each of these mechanisms will be presented in this chapter. To begin a brief description of each of these mechanisms is given.

The rate of radiative damping is governed by the radiative lifetime τ_0 of the upper level of the clock transition. In frequency standards this lifetime can be between a hundred milliseconds for an optical transition and many years for a microwave standard. The effect of the radiative lifetime is to set an effective limit on the maximum possible interrogation time and hence on the stability of the standard. As opposed to optical dephasing, radiative damping is associated with a change in population.

Optical dephasing or decoherence is a decay in the coherence between electronic states without population transfer. Optical dephasing causes the Rabi oscillations to 'wash out', broadening the reference transition. Mechanisms resulting in dephasing include: variation in the Rabi frequency; (laser intensity, laser phase) and clock transition frequency/phase (elastic collisions, Zeeman and Stark shifts, Doppler shifts *etc.*). The term *optical* dephasing applies equally to microwave transitions, but is distinct from *motional* dephasing.

Motional dephasing (*i.e.* motional decoherence) is only present in the motional states of an atom in a harmonic potential, hence is only observed in ion trap standards. Motional dephasing is the analogous effect of optical dephasing, except with the motional states of the atom rather than the electronic states. The decoherence rate is the rate at which the phase between a superposition of motional states becomes random. Distinct from motional heating, no change in the population of the motional state occurs. There is a great deal of discussion in the literature about motional decoherence rates as they are of particular importance to the demonstration of quantum logic gates. Dephasing of the Rabi oscillations occurs in the same way as for optical dephasing, but via fluctuations in the harmonic oscillator energy separations. Time dependent shifts in these separations due to fluctuations in the amplitude and phase of the trapping potential are major contributors to the decoherence rate. As ion trap standards are based on transitions that do not involve motional state transfer, motional decoherence is of less importance than the previous

two effects described.

Motional heating is again only observed in ion traps, whereby the motional state of the ion increase in a dark trap. This mechanism is caused by the dissipation of the fluctuations that cause dephasing via a thermal reservoir. Motional heating is of secondary importance in an optical frequency standard as the atomic reference frequency is insensitive to the ion motion. However if the ion were to be heated out of the Lamb-Dicke regime in a dark trap, it would cause a degradation in performance. The prime mechanism responsible for the motion heating has not been fully determined but is thought to be due to fluctuating trapping fields.

3.1 The modified Optical Bloch equations

The effect of population decay and decoherence is introduced into the optical Bloch equations in the following way [19]:

$$\dot{\rho}_{22} = -i\frac{b^*}{2}\rho_{12}e^{i(\omega_0-\omega)t} + i\frac{b}{2}\rho_{21}e^{-i(\omega_0-\omega)t} - \rho_{22}\gamma_{\text{long}} \tag{27}$$

$$\dot{\rho}_{12} = i\frac{b}{2}(\rho_{11}-\rho_{22})e^{-i(\omega_0-\omega)t} - \rho_{12}\gamma_{\text{trans}} \tag{28}$$

Comparing to equations 3 and 4 shows that the decay and decoherence has been included by the addition of a decay term in both the diagonal and off-diagonal matrix elements. The two decay rates γ_{long} and γ_{trans} are the longitudinal and transverse decay rates respectively. The role of each of these decay constants will be discussed shortly. The introduction of these decay terms causes the solutions to no longer be oscillatory, but instead settle to some steady state value after a sufficiently long time. The effects of radiative decay and decoherence on the atomic line shape can be understood by plotting ρ_{22}, the population of the clock state as a function of frequency ω for various values of γ_{long} and γ_{trans}.

3.2 Radiative Damping

The first case to consider is that of purely radiative damping. In this case:

$$\begin{aligned} \gamma_{\text{long}} &= 2\gamma_0 \\ \gamma_{\text{trans}} &= \gamma_0 \end{aligned} \tag{29}$$

where γ_0 is the radiative decay rate of the clock state which is related to its lifetime τ_0 by $\gamma_0 = 1/2\pi\tau_0$. Note that even in the complete absence of additional decoherence, there is still an off-axis decay rate.

To understand the effect of radiative decay on the stability of the standard, it is desirable to solve equations 27 and 28 to give an expression for the population of the clock state ρ_{22} as a function of frequency. This would enable an expression for the atomic error signal slope to be derived. It is, however, not possible to write a general analytic expression, thus the problem must be solved numerically.

Before this solution is discussed, some insight is gained by considering the case of zero detuning $\omega = \omega_0$. With the initial conditions $\rho_{22} = 0$ and $\rho_{12} = 0$ [19]:

$$\rho_{22} = \frac{\frac{1}{2}|b|^2}{2\gamma_0^2 + |b|^2}\left\{1 - \left[\cos(\lambda t) + \frac{3\gamma_0}{2\lambda}\sin(\lambda t)\right]\exp(-3\gamma_0 t/2)\right\} \tag{30}$$

where $\lambda = \sqrt{|b|^2 - \gamma_0^2/4}$.

It can be seen that the term in square brackets in equation 30 oscillates, giving the usual optical nutation. Indeed if γ_0 is set to zero we regain the expression for Rabi oscillations of equation 7. The oscillating term is exponentially damped by the radiative decay. The Rabi oscillation therefore only occurs for $b \ll \gamma_0$. For π pulse interrogations $bt_{\text{int}} = \pi$ thus optical nutation only occurs for interaction times much less than the radiative lifetime $t_{\text{int}} \ll \tau_0$. Figure 8 plots the excitation probability ρ_{22} as a function of time for various radiative decay rates. The probability of excitation rapidly falls off as the interaction time approaches, and exceeds, the radiative lifetime and hence the slope of the atomic error signal also diminishes. This will lead to a rapid reduction in the stability of the frequency standard. For $t_{\text{int}} \gg \tau_0$ the process is akin to continuous excitation and no oscillation in the population is observed.

Figure 9 shows numerical solutions to the optical Bloch equations (equations 27 and 28). The Mathematica routine to calculate these line shapes was kindly provided by Dr Christian Tamm of the Physikalisch Technische Bundesanstalt (PTB) of Germany.

In these plots one sees how the line shape of the transition changes as t_{int} approaches $1/\gamma_0$. In each case the pulse area has been set to π, applicable for rectangular pulses. For $t_{\text{int}} \ll 1/\gamma_0$ the width of the central component of the line shape is Fourier transform limited and therefore given by $\Delta\omega \sim 1/t_{\text{int}}$. As t_{int} is increased, so the width of the transition is reduced. Here the probability of absorption at line centre is close to unity. As t_{int} approaches and exceeds $1/\gamma_0$, the probability rapidly diminishes as also described by equation 30. In addition the width $\Delta\omega$ of the transition is no longer significantly reduced. This reduction in transition probability coupled with no further reduction in width has a detrimental effect to the stability of the standard via the atomic error signal slope (C_0 in equation 26). Comparing the plot of the Rabi oscillations and these plots of the atomic line shapes, one sees the correlation between a reduction in the Rabi oscillations and a reduction in the error signal slope. Estimating from the plots in figure 9 the optimum interrogation time appears to be around $t_{\text{int}} \sim \gamma_0$.

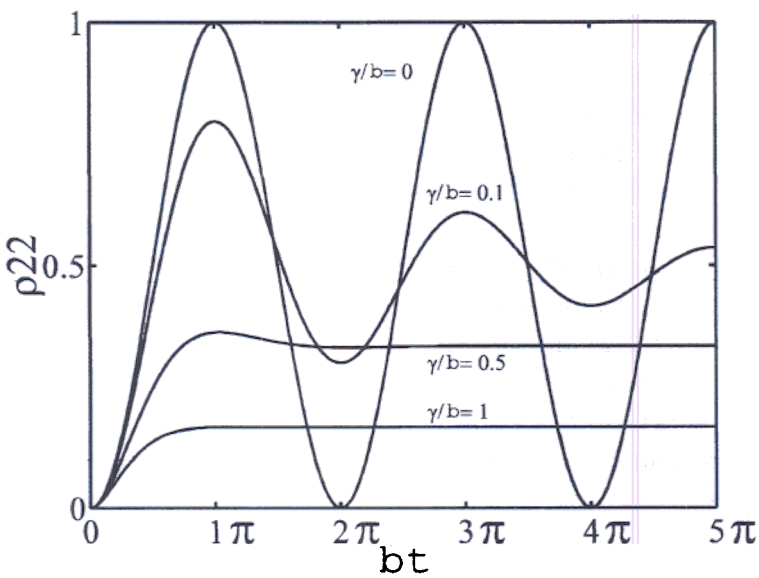

Figure 8: Rabi oscillations in the case of finite radiative decay
Transition probability is plotted for case of $\omega = \omega_0$ and various ratios of Rabi frequency to radiative damping rate. For $\gamma = 0$ one obtains pure optical nutation.

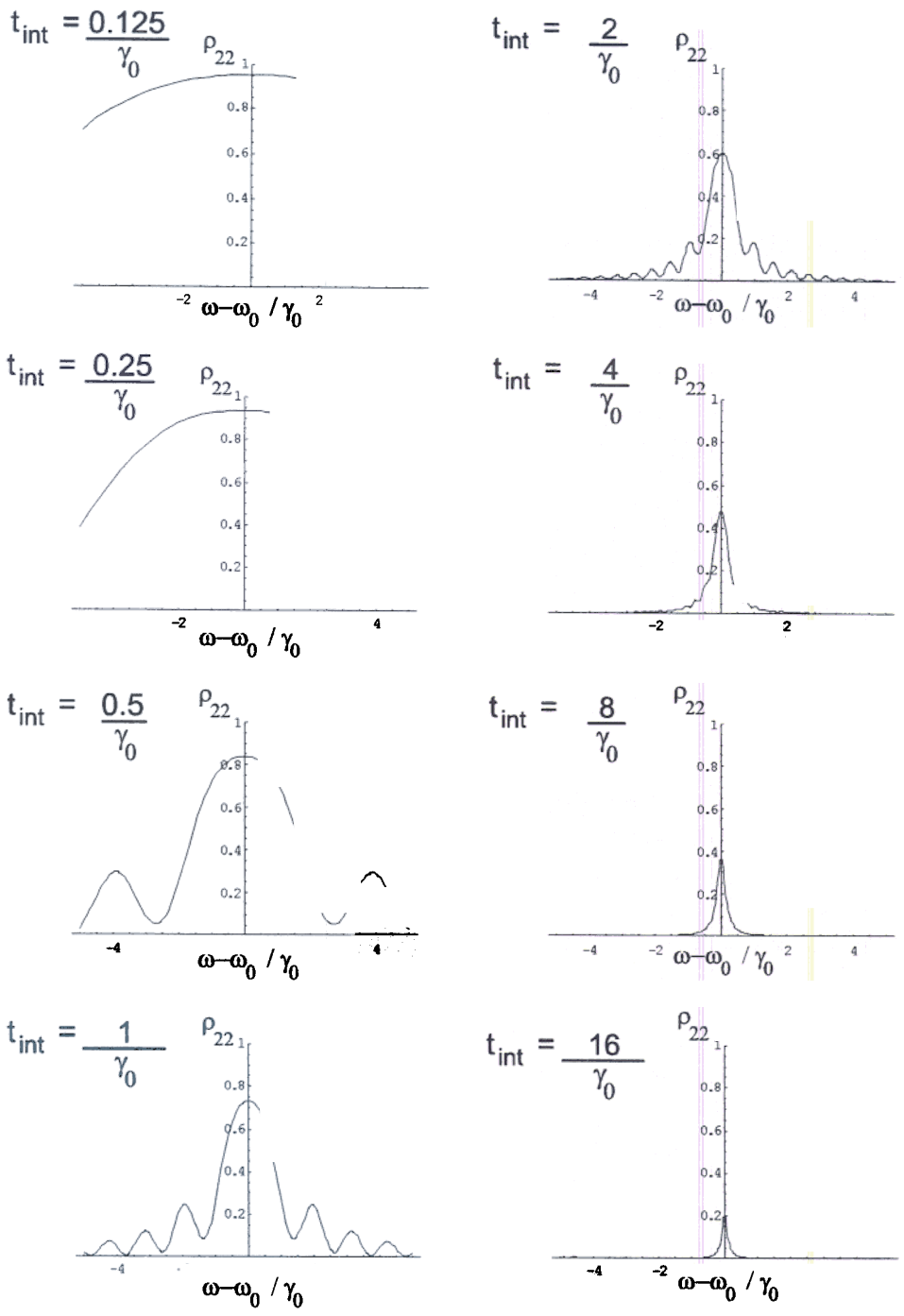

Figure 9: Case of purely radiative decay

Here $\gamma_{\text{transverse}} = \gamma_{\text{longitudinal}}/2 = \gamma_0$. Plot of the excitation probability ρ_{22} as a function of frequency. Shows the line shape observed for various interaction times in the region where the interaction time is close to the upper state lifetime. Note that as the interaction time approaches and exceeds the natural lifetime of the upper state, the excitation probability at line centre rapidly diminishes, thus reducing the stability of the standard.

3.3 Optical Dephasing / Decoherence

Decoherence is

> ...dephasing due to processes that cause random phase changes whilst preserving the population of the atomic levels. Important mechanisms that result in dephasing effects are collisions, stray fields, and laser instabilities *Huelga et al.* [25].

The term optical decoherence denotes dephasing of the electronic or hyperfine levels of an atom as opposed to its motional states. In terms of the optical Bloch equations, dephasing is treated by making the transformation in equation 28:

$$\gamma_{trans} \Rightarrow \gamma_0 + \gamma_{\rm dec} \tag{31}$$

where $\gamma_{\rm dec}$ is the decoherence rate (*e.g.* the elastic collision rate).

As before, it is not possible to write out an explicit solution to the optical Bloch equation, making numerical methods necessary. However the special case where the transverse damping rate is much larger than the longitudinal ($\gamma_{\rm trans} \gg \gamma_{\rm long}$) enables one to set $\gamma_{\rm long} = 0$. This special case has been treated by Huelga *et al.* [25] and will be discussed in the next section. Subsequently the numerical solutions are presented.

3.3.1 Stability for $\gamma_{\rm long} = 0$

Consider ordinary Ramsey interrogations in the absence of any population decay. This case is of relevance for experiments involving purely hyperfine levels as the clock states, but is not applicable for most optical transitions.

As on page 10, consider a two pulse Ramsey interrogation of free precession period $t_{\rm int}$ yields a probability of exciting the clock transition of:

$$P = (1 + \cos(\omega - \omega_0)t_{\rm int})/2. \tag{32}$$

This gives the usual equation for the quantum projection noise of equation 2.

Next the case of an off-diagonal damping term is considered. Here it is still assumed that the radiative decay rate is negligible but a decoherence decay rate of $\gamma_{\rm trans} = \gamma_{\rm dec} = 1/\tau_{\rm dec}$ is important. This also involves setting $\gamma_{\rm long} = 0$ in equation 27 (*i.e.* $\gamma_{\rm trans} \gg \gamma_{\rm long}$). The effect of the off-diagonal damping term is to decohere the signal:

$$\rho_{22} = \left[1 + \cos\left\{(\omega - \omega_0)t_{\rm int}\right\} e^{-\gamma_{\rm dec} t_{\rm int}}\right]/2 \tag{33}$$

As a result of the decoherence the optical nutation decays away with a characteristic time $\tau_{\rm dec}$ to a value of 1/2 (see figure 10). It is easy to see from equation 33 that for $t_{\rm int} \ll \tau_{\rm dec}$ then $e^{-\gamma_{\rm dec} t_{\rm int}} \sim 1$ and the usual Rabi oscillations occur. However for

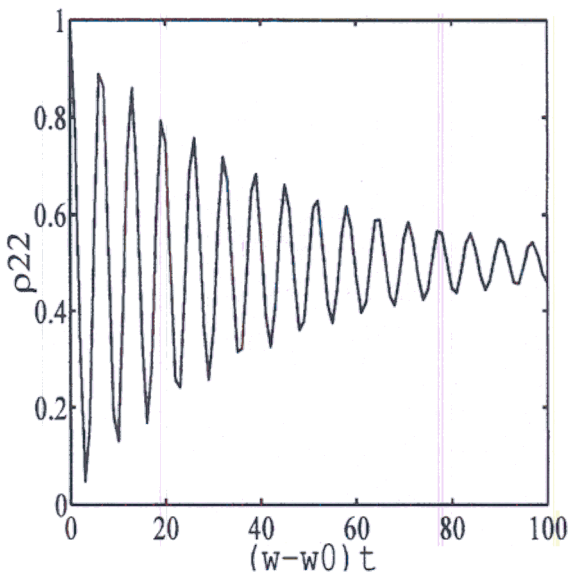

Figure 10: The inclusion of a decay term in the off axis matrix element of the optical Bloch equations causes the Rabi oscillations to decay

$t_{\text{int}} > \tau_{\text{dec}}$ the optical nutation disappears, which as we will see also means that the slope of the error signal and therefore the stability of the standard are reduced.

Huelga *et al.* goes on to show that the effect on the standard's stability is to change equation 2 to

$$\sigma_y(\tau) = \frac{1}{\omega_0}\sqrt{\left(\frac{1}{Nt_{\text{int}}\tau}\right)\left(\frac{1-\cos^2[(\omega-\omega_0)t_{\text{int}}]e^{-2\gamma_{\text{dec}}t_{\text{int}}}}{e^{-2\gamma_{\text{dec}}t_{\text{int}}}\sin^2[(\omega-\omega_0)t]}\right)} \tag{34}$$

It can be seen that the first term is that of the usual quantum projection noise. The second term degrades the stability of the standard. The minimum value of $\sigma_y(\tau)$ occurs for:

$$\begin{aligned}(\omega-\omega_0)t_{\text{int}} &= k\pi/2 \quad (k \text{ odd}) \\ t_{\text{int}} &= \tau_{\text{dec}}/2\end{aligned} \tag{35}$$

provided $\tau > \tau_{\text{dec}}/2$. Using these conditions gives a minimum stability of:

$$\sigma_y(\tau) = \frac{1}{\omega_0}\sqrt{\frac{2e}{N\tau_{dec}\tau}} \tag{36}$$

Equation 34 is plotted in figure 11 for the condition $(\omega-\omega_0)t = k\pi/2$. It can be clearly seen that the effect of the off-axis decay mechanism causes there to be a minimum in the stability for $t_{\text{int}} = \tau_{\text{dec}}/2$. For $t_{\text{int}} < \tau_{\text{dec}}/2$ increases in interrogation time reduces the width of the transition by a reduction in power broadening. For $t_{\text{int}} > \tau_{\text{dec}}/2$ however, further increases in interaction time result in worse stability due to the decrease in the size of the signal, coupled with little further reduction in the signal width.

These results are only applicable if $\gamma_{\text{trans}} \gg \gamma_0$. This is not usually the case for an optical frequency standard. An exception to this case is the single ion optical frequency standard based on the $^2S_{1/2}$-$^2F_{7/2}$ transition in $^{171}Yb^+$. As the lifetime of the $^2F_{7/2}$ state is around 10 years, the inequality applies. Hence the stability of this standard will purely be limited by the transverse decoherence rate. In a practical system, this is likely to be laser phase and intensity fluctuations with a rate in the range of $\gamma_{\text{dec}} \sim 10^{-2} \rightarrow 1$ Hz.

3.3.2 Stability in presence of population decay *and* dephasing

The results of the previous section are important for the case where the radiative decay probability is negligible. However for most optical frequency standards, this is not this case. The lifetime of the clock state is typically between 10 ms and 1 second. In this case the results of Huelga *et al.* do not hold. Instead it is necessary to numerically solve the optical Bloch equations 27 and 28 to give the probability

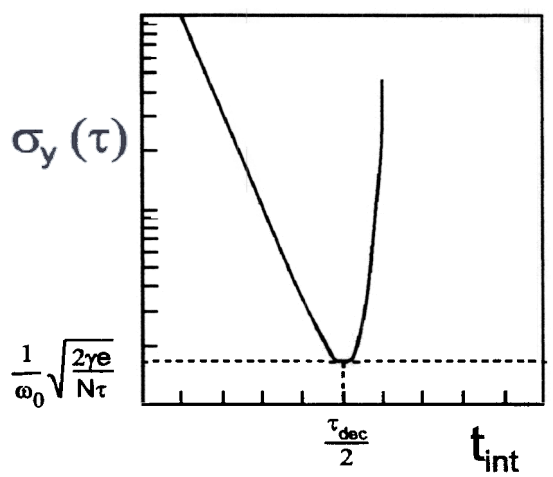

Figure 11: Stability of a frequency standard versus interaction time t_{int} in the case of a transverse decoherence rate of γ (logarithmic axes).

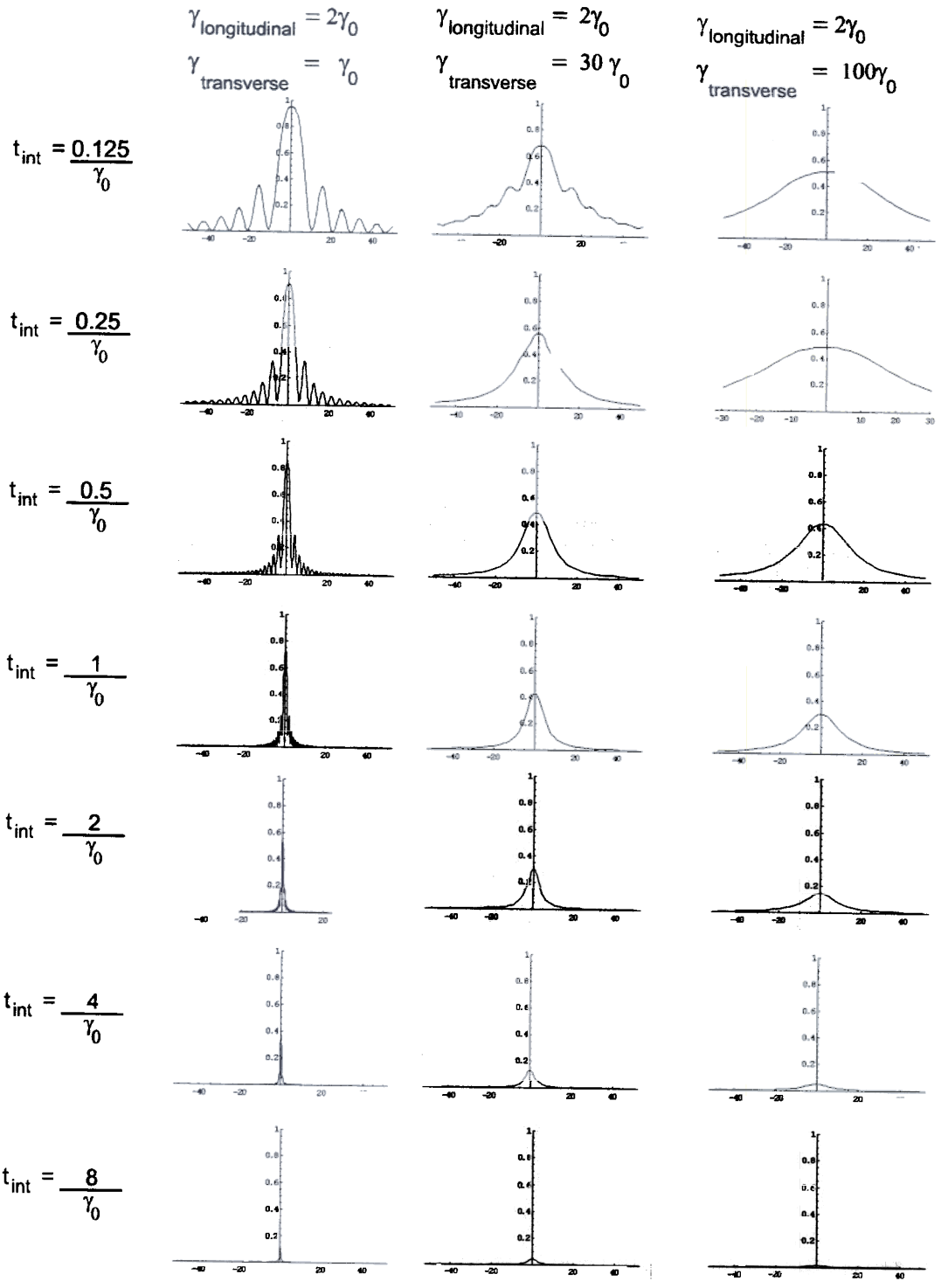

Figure 12: Case of radiative decay and decoherence

Here ρ_{22} of equation 30 is plotted as a function of frequency for various amounts of transverse decoherence.

of excitation ρ_{22} as a function of frequency ω. The results of such a calculation are shown in figure 12.

This figure was again generated using the Mathematica routine kindly provided by Dr Christian Tamm of PTB, Germany. Three cases are plotted in the three columns. The first case is the same as shown in figure 9, and is included for reference. Note the horizontal frequency axis is ten times greater than in figure 9. To recap, this first column shows the evolving line shape obtained for various interrogation times for the case of purely radiative decay (*i.e.* $\gamma_{\text{long}} = 2\gamma_0, \gamma_{\text{trans}} = \gamma_0$). The other two columns show the effect of decoherence, where the transverse decay rate is increased first to $30\gamma_0$ and then $100\gamma_0$. Note that all the plots are scaled with γ_0. As can be seen in the figure, the width of the transition for a particular interrogation time is approximately proportional to the transverse decay rate γ_{trans}. The peak transition probability is also reduced with increasing decoherence. The optimum slope occurs for somewhere around $t_{\text{int}} = 1/\gamma_0$.

The results show a qualitative similarity to those of the case where $\gamma_0 = 0$. The frequency width of the transition decreases as the interrogation time increases (*i.e.* as the Fourier transform limited width decreases). For $t_{\text{int}} \gg 1/\gamma_0$ the signal intensity decreases rapidly without significant reduction in width, reducing the slope of the error signal.

Therefore it can be seen that the performance of a frequency standard is degraded by decoherence. In the presence of radiative decay, the optimum interrogation time is of the order $t_{\text{int}} = 1/\gamma_0$, but the width of the transition is proportional to the transverse decoherence rate t_{dec} of the previous section.

3.3.3 Causes of decoherence / dephasing

Once the link between decoherence rate and stability has been established, it is important to be able to quantify likely sources of decoherence. This raises the question, what are the sources of dephasing? The question can be answered in part by examining the effects of dephasing, and the mechanisms by which the effects come about.

One of the most common sources of dephasing treated in textbooks is that of elastic collisions [19]. Mathematically elastic collisions are treated in the manner described above, that is increasing the transverse relaxation rate to $\gamma_{\text{trans}} = \gamma_0 + \gamma_{\text{coll}}$ where γ_{coll} is the elastic collision rate. The effect of elastic collisions is often explained by the interruption of the coherence between the two atomic states. In this way the phase is reset after every collision. Hence the effective interaction time becomes the mean duration of the coherence between collisions. This model can be used to explain other forms of decoherence.

Another interpretation of this model is to consider the Rabi oscillations of an atom. Any form of dephasing will cause the Rabi oscillations to 'wash out'. A crude

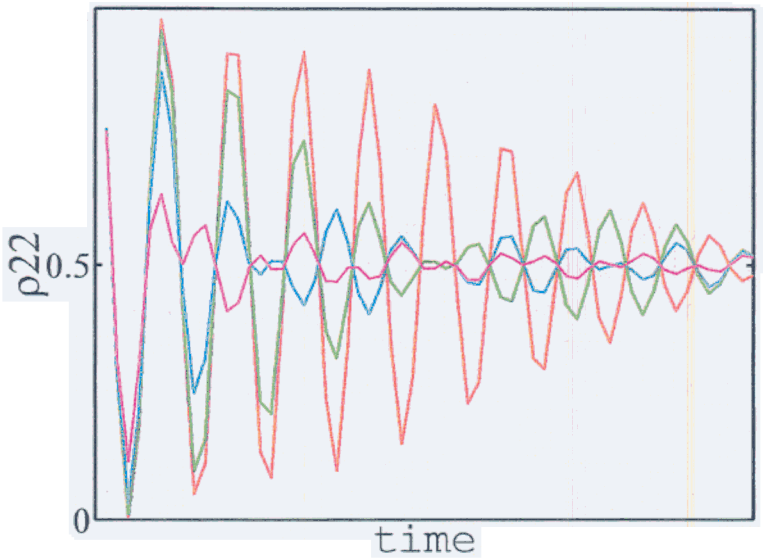

Figure 13: Effect of fluctuating Rabi frequency
Rabi oscillations of equation 6 are plotted for various degrees of fluctuating Rabi frequency. Red = 5% fluctuation, green = 10% fluctuation, blue = 20% fluctuation, magenta = 40% fluctuation

demonstration of the sensitivity of the coherent superposition of states to dephasing can be seen by modelling Rabi oscillations for fluctuating parameters. Figure 13 shows Rabi oscillations for various degrees of fluctuation in the Rabi frequency b. As can be seen, the larger the degree of dephasing the shorter the characteristic dephasing or decoherence time τ_{dec}. Comparing these plots with figure 10 shows a similar behaviour and hence the reduction in stability of equation 34 is to be expected. A more careful study of dephasing due to fluctuating parameters have also been developed [28, 29, 30].

When trying to understand which experimental parameters influence dephasing, one needs to look at the constituents of the oscillation frequency. Equation 6 shows that the oscillation frequency depends on ω, ω_0 and b. Laser phase fluctuations show up in ω whilst intensity fluctuations occur through b. Fluctuations in ω_0 occur via atomic physics limitations. On long time scales these are considered reproducibility issues. On timescales of the order of the interrogation time t_{int} these are more properly considered as stability limitations. Varying magnetic and electric fields can perturb ω_0 via the Zeeman and Stark effects. Elastic collisions are also treated as a dephasing source.

All is not lost, as in frequency standards there is a degree of protection from these effects by choosing a perturbation free environment or an atom which is to a degree insensitive to such things as stray fields. In the case of an ion trap standard based on a single ion, the dependency of the carrier frequency to atomic frequency perturbations is small. An insight into the magnitude of the dephasing effects can be obtained by considering the analogous case of a microwave frequency standard. In the case of ion trap microwave frequency standards, Ramsey fringes are visible even for interrogation times of $t_{\text{int}} > 100$ s [24, 12]. This leads one to predict that in a single ion optical frequency standard, the optical dephasing decay time τ_{dec} will not be significantly less than 100 seconds. This leads one to predict that it will be radiative decay that is the main limitation to the stability of a single ion optical standard. However, it is important to note that this argument assumes the interrogating laser in the optical standard will introduce no more dephasing effects than the high purity microwave sources used in the microwave standard. This is not an altogether reasonable assumption given that the laser is operating at a frequency in excess of 10 000 times higher than that of the microwave sources. However, this is an area of very active research [31, 32]. It is likely that lasers with line widths in the range 1 Hz down to 10 mHz may be possible to realise soon.

3.4 Motional Dephasing and Damping

As quantized motional effects occur only in a harmonic potential so the effect of motional dephasing is only of interest in some form of trap potential. By far the most common trapping potential used is that of the Paul trap and hence the discussion here will be limited to this case [33, 34].

The effects of motional dephasing can be described with exactly the same formalism as for optical dephasing. In fact motional decoherence has little importance for frequency standards work, but a large amount of literature has been devoted to the subject [35, 28, 29, 36, 37] due to its importance in the field of quantum information processing (*i.e.* quantum computation [38]).

An ion trap sets up a (near) harmonic potential in which an ion resides. In the case of a Paul trap this is a pseudopotential well. This forms a quantum harmonic oscillator, with quantized motional states spaced by the harmonic potential frequency ω_ν. For a tightly bound atom the motional energy is given by $E = \hbar\omega_\nu(n+\frac{1}{2})$, where n is the vibrational quantum number (see figure 14). The motional decoherence rate is the rate at which the phase between a superposition of n and $n+1$ vibrational states become random [30]. The ion is held in the Lamb-Dicke regime [39]. In this case the absorption spectra of the ion consists of a main carrier at $\omega = \omega_0$ and a number of motional sidebands spaced by the secular frequency of the trap ω_ν. The sidebands for the 3 dimensions (x, y and z) are not necessarily degenerate. The first order upper sidebands at $\omega = \omega_0 + \omega_\nu^{x,y,z}$ correspond to a transition which increase

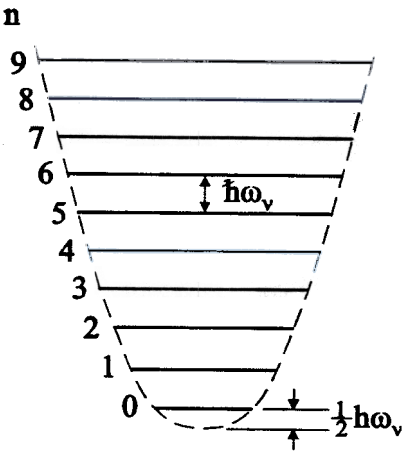

Figure 14: Harmonic potential well for a Paul trap.
The ladder potential is made up of n motional states spaced by $\hbar\omega_\nu$, where ω_ν is the secular frequency of the trap.

the motional quantum number n by one quanta, and the lower sidebands reduce n by one quanta.

The reference transition for the frequency standard is obtained by driving the carrier transition. This corresponds to a transition in which the motional state of the ion remains unchanged. For this reason there is no interaction with the motional state of the ion and hence the carrier transition is unaffected by motional decoherence.

This fact is clearly demonstrated in a microwave frequency standard. Again the carrier transition is used as the frequency reference. A typical spectrum of a microwave transition shows a very narrow carrier and relatively broad motional sidebands [24]. This is because the side bands are broadened by the decoherence effect described, whilst the carrier is unaffected.

The motional decoherence or dephasing occurs in an analogous way to optical decoherence. Any mechanism which perturbs the motional ladder states spacing will cause the motional state to decohere. Hence anything which changes the secular frequency of the ion ω_ν will decohere its motional state. The secular frequency of the ion is related to the trap drive frequency Ω_{RF} and the Lamb-Dicke parameter β by:

$$\omega_\nu = \frac{1}{2}\beta\Omega_{\mathrm{RF}} \tag{37}$$

Hence the dephasing rate has dependencies on the drive frequency and the Lamb-Dicke parameter, which in turn is related to such experimental parameters as the drive voltage and trap size [33, 34]. It is often this set of parameters that is blamed for the high motional decoherence rates observed in traps [35, 37], although to date no full study of these effects has been completed.

So far the discussion of motional effects has been restricted to that of motional decoherence (dephasing). In this case the coherence between different motional state changes with time without effecting the value of n. In addition there is also the motional heating rate which is defined as: the rate at which a trapped ion vibrational (harmonic oscillator) state n is driven to the $n = n + 1$ state due to coupling with a thermal reservoir [30]. This coupling to a thermal reservoir can theoretically cause cooling as well as heating, although for the case of an ion in a low vibrational quantum state it is usually heating. Recently a number of papers have theoretically explored the mechanisms for motional heating and decoherence [30, 40]. This general formalism whereby heating or cooling is caused by fluctuations is known as the 'fluctuation dissipation theorem' (see for example reference [20] page 345).

The heating of the ion in the (dark) trap is of no great consequence for the same reasons that motional decoherence does not effect the carrier transition of the reference. However it would be an issue if the heating rate were so severe that the ion was heated outside the Lamb-Dicke regime during the course of the clock interrogation. As an example of such a heating rate, a string of mercury ions were observed to heat to 25 mK during a 100 s clock interrogation of the NIST mercury ion trap standard [12]. It may be that this heating rate will form a limitation to the maximum possible interrogation time.

Motional decoherence and heating rates are of great interest in state-of-the-art quantum state manipulation experiments. The prerequisite for many of these experiments is to cool an ion to the motional ground state of the trap ($n = 0$). This can not usually be achieved by Doppler cooling alone, but also requires sideband [41] or Raman cooling [42] steps as well. In a pioneering experiment, NIST cooled a single mercury ion to the motional ground state (*i.e.* $n = 0$) [41]. This was achieved by cooling the ion by repeatedly driving the lower motional sideband (sideband cooling). In this experiment a motional heating rate of 6 quanta/second was observed.

In equally impressive experiments at NIST [35, 37] a single beryllium ion was cooled to the ground state. From here non-classical states of motion were created by performing Jaynes-Cumming type interactions via the application of external light fields. In the example of Fock state generation, the ion was manipulated such that its motional state was a pure vibrational quantum number. Once this Fock state had been created the evolution of the motion of the ion could be monitored. It was seen that a pure Fock state decohered at a rate of around 1 kHz. The causes for the heating rates were ascribed, by the authors, to stray fields. However more research will be required if the exact source of the heating and dephasing is to be discovered.

The observed motional heating rates of ~ 1 kHz would be of grave consequence to a frequency standard if they had any effect on it. As was seen in section 3.3 a decoherence rate of 1 kHz would lead to line widths of that order and stabilities described by equation 36. Obviously in a conventional frequency standard the ion

is prepared in a thermal distribution of motional states. The exact distribution depends on the temperature achieved by Doppler cooling. To reiterate, the carrier excitation of the reference transition leaves the ion in the same thermal distribution, hence is not effected by any motional effects.

4 Conclusion

This report has investigated the atomic and measurement limitations to achieving high stability in an optical frequency standard. In particular the case of a standard based on a single ion has been discussed.

In the absence of radiative decay or decoherence, the atomic line shape observed is given by the Fourier transform of the interrogating radiation pulse. This is provided that the pulse area has been properly set ($bt = \pi$ for a rectangular pulse and two pulses of $bt = \pi/2$ for Ramsey interrogation). In this case the quantum projection noise limited stability is given by the commonly quoted formula:

$$\sigma_y(\tau) = \frac{\delta\omega_{\text{rms}}}{\omega_0} = \frac{1}{\omega_0\sqrt{N t_{\text{int}}\tau}}. \tag{38}$$

This shows that longer interrogation times t_{int} gives narrower atomic linewidth and hence better stability.

The quantum projection noise limited stability of equation 38 is the fundamental lower limit of the stability of a frequency standard. In practice a number of factors conspire to reduce the stability of the standard. Most fundamentally these are radiative damping and optical (or electronic) decoherence. In the case of a microwave frequency standard, where the radiative damping rate is negligible and electronic decoherence is low, quantum projection noise limited stability can be achieved [7].

For most optical systems, radiative decay is non-negligible and optical dephasing/decoherence common. The effect of this is to degrade the stability. A crude analysis shows that the stability of the system is governed by the slope of the atomic error signal shown in equation 26. This gives the almost intuitive result that the stability of the standard is proportional to the width of the reference transition. The effect of radiative decay and dephasing can be studied by solving the optical Bloch equations (equation 27 and 28). A numerical simulation of this shows how the signal size (and hence error signal slope) reduces as the interrogation time approaches and then exceeds the decay rate. The effect of additional decoherence can be modeled by increasing the transverse decay rate $\gamma_{\text{transverse}}$. This shows that for $\gamma_{\text{trans}} \gg \gamma_0$ the width of the reference transition was roughly proportional to the transverse decay rate, and hence so is the stability.

The radiative decay rate for a system is set by the upper state lifetime of the transition and is therefore fixed for a particular element. The transverse decay rate is given by effects which homogeneously broaden the linewidth of the atomic reference transition. These include elastic collisions, laser phase and intensity fluctuations and Zeeman, Doppler and Stark shifts. In an ion trap system where the atomic reference frequency is largely insensitive to the effects of varying external fields (magnetic and electric) the predominant cause of dephasing is expected to be laser phase and frequency fluctuations. A great deal of research is going into reducing

these effects [32, 31].

Another decoherence source, motional dephasing, has received a great deal of interests in the literature [35, 28, 29, 36, 30, 37, 25]. This describes the loss of coherence in an individual motional state of an ion trap harmonic oscillator. This effect is therefore not present in systems such as atomic fountains or beam standards. The harmonic oscillator level spacings of such motional states are governed by the trap potential voltage and frequency. Any fluctuation in these parameters leads to decoherence of the motional Fock states [35, 37]. The exact source of the dephasing is not well understood [37], but is observed to be in the range of 100 Hz to a few kilohertz [42].

However in a frequency standard it is unlikely that an individual Fock state will be used. Instead a thermal distribution of motional states is set up due simply to Doppler cooling the ion to the Lamb-Dicke regime. The absorption spectrum of an ion in a strongly binding trap shows a carrier and secular sidebands due to the motion of the ion. A frequency standard relies on driving this carrier transition which is free from the first order Doppler effect. It is this independence of the carrier to the ion's motion which make it insensitive to motional dephasing effects. This is fortunate as dephasing on millisecond timescales and of unknown origin would be of great concern to a metrologist. It remains a major hurdle to the realisation of a quantum computer.

The fact that motional decoherence is of little relevance to frequency standards can be seen from the ion trap microwave standard case. Microwave standards have been studied for many years and yield excellent stabilities [24, 12]. Microwave spectra show extremely narrow carrier transitions which are used for stabilising the microwave oscillator. In addition broad motional sidebands can also be observed [24]. The width of these sidebands is governed by heating rates and motional decoherence. As free precession Ramsey interrogation times as long as 100 seconds are commonly used [24, 12, 43], the sensitivity to any decoherence rate would be pronounced. The insensitivity to motional decoherence is clear from this case. As for dephasing of the hyperfine levels (optical dephasing), it is fairly clear that this is also not an extreme problem. At UHV pressures elastic collisions occur on the tens of seconds time scale [5], Zeeman shifts are minimised by driving field insensitive transitions and by using magnetic shielding. Doppler and Stark fluctuations are intrinsically low. Phase and intensity fluctuations of the microwave source contribute somewhat to the overall decoherence rate, yet are much better controlled than their optical analogue - the laser. In the case of microwave standards then, stabilities tend to be limited by interrogation time and possibly heating of the ions in the dark trap.

The outlook for the stability single ion optical frequency standard appears good. Provided that laser sources of sufficiently low phase noise ($\ll$ 1 Hz) and intensity noise can be constructed there is no reason why transitions with stabilities limited by the radiative lifetime of the upper clock state can not be achieved. An interesting

exception to this is the 467 nm $^2S_{1/2}$-$^2F_{7/2}$ (F=0 – F=3, m_F=0) transition in $^{171}Yb^+$ [18]. The 10 year lifetime of the $^2F_{7/2}$ state makes radiative decay a negligible contributor to the overall decoherence of the ion. Again, provided that a laser source of sufficient stability can be developed, the possibility of interrogation times greatly in excess of 1 second seem a reality. Even at only t_{int}=1 s, a projection noise limited stability of $\sigma_y(\tau) = 2 \times 10^{-16}\tau^{-1/2}$ is attained, reducing to $\sigma_y(\tau) = 8 \times 10^{-17}\tau^{-1/2}$ for $t_{int} = 10$ s.

It is clear from the discussion of this report that experiments which investigate the magnitude and sources of decoherence in optical frequency standards would be of great interest. This goal could be achieved by measuring the decay rate of Rabi oscillations, in addition to actually measuring the stability achieved for the standard. In this way it would be hoped that technical sources of decoherence could be identified and reduced. For the field of quantum information processing, the identification and elimination of motional decoherence effects is an even more urgent requirement.

The projected stabilities for single ion optical frequency standards suggest that it will be possible to achieve stabilities in excess of $10^{-15}\tau^{-1/2}$. This will enable the uncharted waters of reproducibility in excess of 10^{-16} to be explored in the near future.

Symbols

This glossary lists the symbols *commonly* used within the text. Other symbols not listed are defined locally within the text. .

y	Dimensionless frequency
ω_0	transition centre frequency [radHz]
ω	laser frequency [radHz]
$\sigma_y(\tau)$	root Allan variance of dimensionless frequency fluctuations
$\delta\omega_0$	uncertainty in value of ω_0 [radHz]
$\Delta\omega$	FWHM of reference transition [radHz]
C_0	signal size
t	time [s]
N	number of atoms(ions)
n	number of measurements
t_{int}	interrogation time [s]
t_r	duration of Ramsey pulse [s]
τ	averaging time [s]
T	single measurement duration [s]
b	Rabi frequency [radHz]
ρ	density matrix element
$\Omega = \sqrt{(\omega_0 - \omega)^2 + b^2}$	[radHz]
FWHM	Full-width-at-half-maximum [radHz] (unless stated otherwise)
$\gamma_{\text{longitudinal}}$	longitudinal decay rate [radHz]
$\gamma_{\text{transverse}}$	transverse decay rate [radHz]
γ_0	spontaneous population decay rate [radHz]
τ_0	clock state lifetime [s]

Acknowledgments

The author would like to acknowledge the support of a number of individuals. Firstly, thanks to Dr Christian Tamm of the Physikalisch Technische Bundesanstalt (Germany) for his patience in discussing his extensive knowledge of this subject and for providing the Mathematica routine used extensively in chapter 3, in addition to answering an endless list of questions by email. Thanks also to Dr Alan Madej of the Institute for National Measurement Standards, National Research Council (Canada) for his enlightening discussions on the subject. Thanks also to Dr Geoff Barwood of NPL for proof reading this report at very short notice, and to Dr Patrick Gill (project manager) for his support during this work and in proposing the report's subject matter.

References

[1] W. Itano and N. Ramsey, Accurate measurement of time, July 1993.

[2] R. Bell, *SI: The international system of units* (HMSO, 1993).

[3] T. Udem *et al.*, Opt. Lett. **24**, 881–883 (1999)

[4] J. Bernard *et al.*, Phys. Rev. Lett. **82**, 3228-3231 (1999)

[5] A. Madej and J. Bernard, in *Topics in applied physics*, edited by A. Luiten (Springer, 1999).

[6] J. L. Hall *et al.*, pp. 267–276, in [44]

[7] G. Santarelli *et al.*, Phys. Rev. A **82**, 4619–4622 (1999).

[8] D. W. Allan, IEEE Trans. Ultrason. Ferroelec. Freq. Contr. **34**, 647–654 (1987).

[9] D. W. Allan, Proc. IEEE **54**, 221–230 (1966).

[10] *NIST Technical Note "Characterisation of Clocks and Oscillators"* (US Govt Printing Office, 1990), Vol. 1337.

[11] D. J. Wineland *et al.*, pp. 71–77, in [45]

[12] D. J. Berkland *et al.*, Phys. Rev. Lett. **80**, 2089–2092 (1998).

[13] H. Dehmelt, IEEE Trans. Instrum. Meas. **31**, 83–87 (1982)

[14] G. Barwood *et al.*, Phys. Rev. A **59**, R3178-R3181 (1999)

[15] D. Engelke and C. Tamm, Europhys. Lett. **33**, 347–352 (1996).

[16] C. Tamm and D. Engelke, in *Laser Spectroscopy XIII*, edited by Z.-J. Wang, Z.-M. Zhang, and Y.-Z. Wang (World Scientific, 1998), pp. 180–182.

[17] C. Gerz *et al.*, Z. Phys. **D8**, 235–237 (1988).

[18] M. Roberts *et al.*, Phys. Rev. Lett. **78**, 1876–1879 (1997).

[19] R. Loudon, *The Quantum Theory of Light*, (Oxford University Press, 1983, 2nd ed.)

[20] G. G. C Cohen-Tannoudji, J. Dupont-Roc, *Atom-photon interactions* (John Wiley and Sons, Inc, 1992).

[21] G. K. Woodgate, *Elementary Atomic Structure*, (Oxford University Press, 1983, 2nd ed.).

[22] N. Ramsey, Phys. Rev. **76**, 996 (1949).

[23] N. Ramsey, *Molecular Beams* (Oxford University Press, 1956)

[24] P. Fisk, Rep. Prog. Phys. **60**, 761-817 (1997)

[25] S. Huelga *et al.*, Phys. Rev. Lett. **79**, 3865–3868 (1997)

[26] D. J. Wineland *et al.*, Proposed stored $^{201}Hg^{+}$ ion frequency standards, 1981

[27] W. Itano *et al.*, Phys. Rev. A **47**, 3554–3570 (1993).

[28] S. Schneider and G. Milburn, Phys. Rev. A **57**, 3748–3752 (1998)

[29] M. Murao and P. Knight, Phys. Rev. A **58**, 663–669 (1998)

[30] S. Lamoreaux, Phys. Rev. A **56**, 4970–4975 (1997)

[31] B. Young *et al.*, Phys. Rev. Lett. **82**, 3799–3802 (1999)

[32] M. Roberts, P. Taylor, and P. Gill, *Laser linewidth and the sub-hertz level* (NPL, 1999), Vol. CLM 8.

[33] H. Dehmelt, Adv. At. Mol. Phys. **3**, 53–72 (1967)

[34] D. J. Wineland, W. M. Itano, and R. S. V. D. Jr, Adv. At. Mol. Phys. **19**, 135–186 (1983).

[35] D. Meekhof *et al.*, Phys. Rev. Lett. **76**, 1796–1799 (1996)

[36] R. Omnès, Phys. Rev. A **56**, 3383–3394 (1997).

[37] C. Monroe *et al.*, Science **272**, 1131–1136 (1996)

[38] J. Cirac and P. Zoller, Phys. Rev. Lett. **74**, 4091–4094 (1995).

[39] W. E. Lamb, Phys. Rev. **A51**, 187–190 (1937), this paper is often cited as Lamb's contribution to the "Lamb-Dicke regime". Its relevence is not imediatly apparant, since it deals with neutron capture by a proton. The key point however is Lamb treats the case of a *bound* proton.

[40] S. Sceider and G. Milburn, Phys. Rev. A **59**, 3766–3774 (1999)

[41] F. Diedrich *et al.*, Phys. Rev. Lett. **62**, 403–406 (1989), also in [46]

[42] C. Monroe *et al.*, Phys. Rev. Lett. **75**, 4011–4014 (1995), also in [47].

[43] C. Tamm, D. Schnier, and A. Bauch, Appl. Phys. **B60**, 19–29 (1995).

[44] in *Proceedings of the 5th Symposium on Frequency Standards and Metrology*, edited by J. C. Bergquist (World Scientific, 1996).

[45] in *Proceedings of the 4th Symposium on Frequency Standards and Metrology*, edited by A. De Marchi (Springer-Verlag, 1989).

[46] *NIST Technical Note* (US Govt Printing Office, 1992), Vol. 1353.

[47] *NIST Technical Note* (US Govt Printing Office, 1996), Vol. 1380.